Fabrication of Copper Patterns on Flexible Substrate by Patterning–Adsorption–Plating Process

Yu Chang, Chao Yang, Xin-Yao Zheng, Dong-Yu Wang, and Zhen-Guo Yang*

Department of Materials Science, Fudan University, Shanghai, P.R. China

Ⓢ *Supporting Information*

ABSTRACT: A novel patterning–adsorption–plating process to additively fabricate copper patterns is developed. Functional ink with ion-adsorption nanoparticles was inkjet printed on PET substrate to form the patterned adsorption film. Catalytic ion was adsorbed by amino groups in the adsorption film, and catalyzed the electroless plating of copper. The mercapto groups introduced to the film enhance the reliability of the patterns. Specific solvent used in the ink increase the surface roughness of the adsorption film, leading to a better adhesion of the patterns. The prepared copper patterns show excellent conductivity about the same with bulk copper and good adhesion on PET.

Inkjet Printing   Ion-adsorption and Electroless Plating

KEYWORDS: *copper patterns, inkjet printing, ion adsorption, electroless plating, flexible substrate*
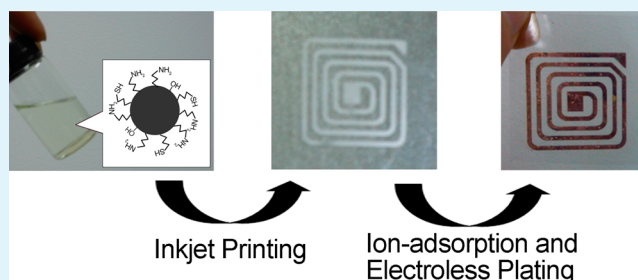
■ INTRODUCTION

Fabrication of conductive patterns by printed electronics has generated growing interest in recent years, and can be applied in the manufacture of printed circuit board (PCB), flexible printed circuit board (FPC), and integrated circuit (IC).[1−12] Compared with the conventional lithography and etching process, printed electronics enjoys the advantages of less wastage of materials, fewer process steps, less pollution, and lower cost.

Inkjet printing of nanoparticles conductive ink is widely researched in the additive fabrication of conductive circuit.[13−19] However, most conductive ink must be printed on heat-resistant substrate for the high sintering temperature. The conductivity of the prepared patterns is far below bulk metal. Besides, copper nanoparticles are easy to be oxidized, thus they must be prepared and sintered without oxygen. These problems increase the cost and limit the applications.

Printing of catalyst ink and metallization by electroless plating is a promising way. This process can be applied on almost all kinds of substrates and does not need inert gas environment. Moreover, the conductivity can be the same with bulk metal.[20−27] But the poor adhesion is the main problem. To guarantee the adhesion, the patterns must be very thin, thus the resistance is large. Surface modification of substrates can enhance the adhesion to a certain degree.[28−31] But the problem still exists when thicker metal is deposited. Another potential method is based on selective adsorption of catalytic ion.[32−36] Ion-adsorption polymer is coated or printed on substrates to form the patterned adsorption film, adsorbing the catalytic ion via complexation or electric charge. Then the patterns are metalized by electroless plating. However, ion-adsorption polymers, which contain amino, carboxyl, quaternary amine

groups or etc., are always water-soluble. The adsorption film will be swelled or dissolved in the electroless plating bath, causing the failure of the patterns. Besides, poor adhesion and large resistance problems still exist. Moreover, the usage of palladium as catalyst increases the production cost.

In this paper, a simple process based on selective adsorption of catalytic ion and electroless plating of copper to fabricate conductive patterns is developed (Figure 1). This method can be called the patterning–adsorption–plating (PAP) process according to the procedures. Ion-adsorption nanoparticles were prepared by hydrolyzing 3-aminopropyltriethoxysilane (APTES) with 3-mercaptopropyltriethoxysilane (MPTES) together. Specific solvent was added to obtain the functional ink. Modified office Inkjet printer was used to print the patterned adsorption film on substrate conveniently. Afterward the substrate was immersed into silver nitrate solution. Silver ion can be adsorbed to the adsorption film via the complexation with amino groups. Finally, the patterns were metallized by electroless plating of copper with the catalyzing of silver. No sintering is needed, so substrates with low heat distortion temperature (HDT) and cost like PET (HDT < 90 °C) can be used. The conductivity of the patterns can be the same with bulk copper. Mercapto groups are introduced to the nanoparticles to enhance the hydrophobicity and stability of the adsorption film. In order to improve the adhesion, we made use of the phenomenon that the crystallization habits of nanoparticles differ in different solvent. The ion-adsorption nanoparticles can crystallize in big particle form when poor
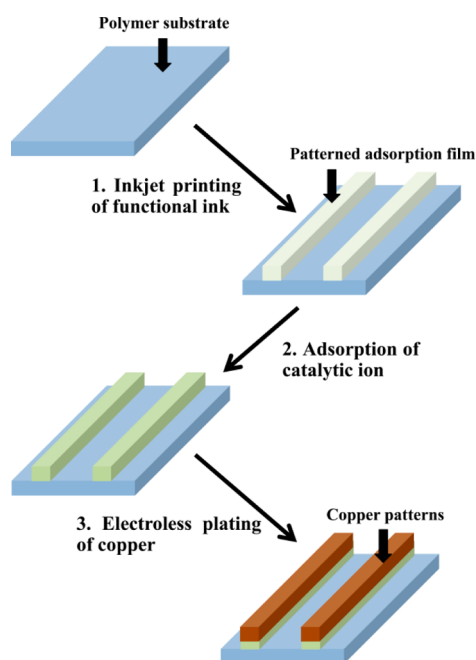
Figure 1. Schematic diagrams of PAP process.

solvent is used. It leads to higher surface roughness of the adsorption film and increase the adhesion of copper patterns.

■ EXPERIMENTAL SECTION

Materials. PET films, ethanol, isopropanol, butanol, 2-methoxy ethanol, butyl acetate, MPTES (99%), silver nitrate, copper sulfate, formaldehyde, potassium sodium tartrate, EDTA disodium, potassium ferrocyanide, sodium hydroxide were all AR grade purchased from Sinopharm chemical reagent Co.,Ltd. APTES (99%) and 2,2′-bipyridyl were AR grade obtained from Shanghai Aladdin reagent company.

Preparation of Functional Ink. APTES (3 g) and MPTES (1 g) were mixed in a sealed flask, then ethanol (0.4 g), isopropanol (0.1 g) and water (0.5 g) were added with stirring at 25 °C for 24 h. Afterward, different solvents (20 g) were added to produce the corresponding functional inks.

Fabrication of Conductive Patterns. A modified office inkjet printer (Epson Me1+) was used to print the patterned adsorption film on PET substrate followed by drying in an oven at 70 °C for 30 min. Afterward, the substrate was put into silver nitrate solution (0.05 M) at 50 °C for 5 s, and rinsed by deionized water. Finally, the substrate was immersed into the copper electroless plating bath comprised of copper sulfate (15 g/L), potassium sodium tartrate (14 g/L), EDTA disodium (19.5 g/L), sodium hydroxide (14.5 g/L), 2,2′-bipyridyl (0.02 g/L), potassium ferrocyanide (0.01 g/L), and formaldehyde (15 mL/L) at 40 °C for metallization. Additional heat treatment at 70 °C for 60 min can relief the internal stress, leading to a better adhesion and stability of the patterns.

Characterization. The Fourier transform infrared spectroscopy (FTIR) images were detected on Nicolet Nexus 470 FT-IR spectrometer. X-ray photoelectron spectroscopy (XPS) was carried out on a RBD upgraded PHI-5000C ESCA system (Perkin-Elmer) with Mg Kα radiation ($h\nu$ = 1253.6 eV). Contact angle was measured on Dataphysics OCA15+ optical contact angle measuring device. The surface profile was measured on Veeco Dektak 150 profilometer. The square resistance was obtained by a four-point probe (Qingfeng, SB100/A, China). SEM (JEOL, JSM-6701F, Japan) was operated at 10 kV to inspect the morphology. TEM (Hitachi, H-600, Japan) sample was prepared by drying the functional ink on copper network. The 3D stereoscopic microscope (Hirox, KH-7700, Japan) was used for optical observation.

■ RESULTS AND DISCUSSIONS

Stability of the Adsorption Film. Ion-adsorption nanoparticles were prepared by hydrolyzing APTES and MPTES together. APTES and MPTES can react with water and generate polysiloxane nanoparticles containing hydroxyl, amino and mercapto groups (Figure 2a) (the size distribution of the
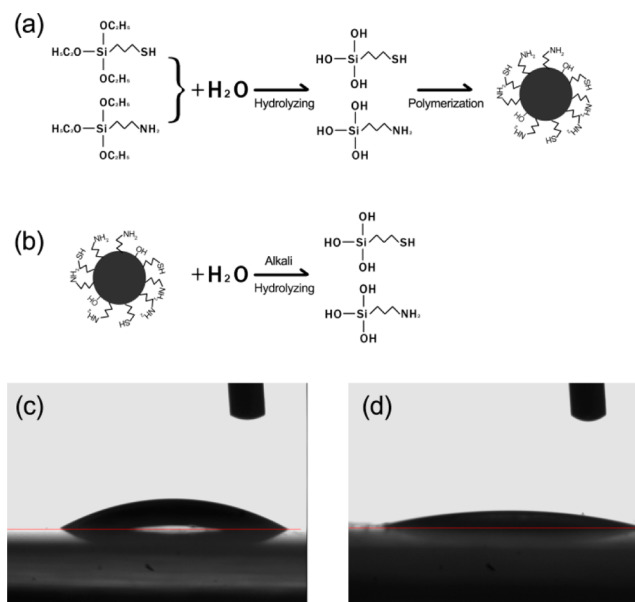

Figure 2. (a) Synthesis process of ion-adsorption nanoparticles. (b) Hydrolyzing of the ion-adsorption nanoparticles in alkaline solution. (c) Contact angle of water on the adsorption film with mercapto groups. (d) Contact angle of water on the adsorption film without mercapto groups.

nanoparticles can be seen in Figure S1 in the Supporting Information). However, polysiloxane can also be hydrolyzed and broken down into small molecules, especially in alkaline solution (Figure 2b). Meanwhile, the adhesion and stability of the adsorption film decline sharply. So, it is very important to prevent the adsorption film from hydrolyzing in the alkaline electroless plating bath.

One solution is to increase the hydrophobicity of the adsorption film. The hydrophobic groups on the surface can block the water from penetrating into the interior. So the hydrolysis of polysiloxane is slowed down, and the adsorption film can maintains stability for longer time. For comparison, the ion-adsorption nanoparticles hydrolyzed only by APTES were prepared. After printed on PET film, the adsorption film was immersed into the electroless plating bath at 40 °C. However, the film was swelled and can be easily shelled off after 10 min. In order to increase the hydrophobicity, mercapto group was introduced. The contact angle of water on the adsorption film with mercapto groups is 30.4° (Figure 2c). Compared to the film without mercapto groups (19.4°) (Figure 2d), the hydrophobicity increases greatly. The hydrophobic adsorption film was also immersed into the electroless plating bath. 30 min later, the film can still be stable and adhere firmly to the substrate. So, the hydrophobic adsorption film can be metalized for longer time, and the conductive patterns with lower resistance are thus obtained.

Relationship between the Solvent and the Adhesion of the Conductive Patterns. The interface of adsorption film and PET substrate is strong. The residual hydroxyl groups on

the nanoparticles can form chemical bonds with carboxyl and hydroxyl groups on the PET substrate. Theoretically, the adsorbed silver ion is reduced to silver nanoparticles by formaldehyde when electroless plating. Mercapo groups can react with silver nanoparticles and form Ag−S bond, thus the catalyst is tightly bonded to the adsorption film. The adhesion between the adsorption film and the deposited copper is related to the surface roughness of the substrates. The enhanced surface roughness leads to better adhesion in a certain range for the film with coarse surface can mechanically anchor the deposited metal tightly. Adding filler particles to the ink can increase the surface roughness of the adsorption film. But, the particles will block the nozzle seriously. So, a novel method was applied to fulfill the requirements of inkjet printing and high surface roughness. It is based on the different crystallization habits of nanoparticles.

Ion-adsorption nanoparticles tend to suspend in solvent with medium polarity, such as ethanol, 2-methoxy ethanol, butanol, etc. Butyl acetate, xylene, etc. with low polarity, are the poor solvent of these nanoparticles. As solvent evaporates, nanoparticles started to crystallize. In the ink with good solvent, nanoparticles tend to separate out and assemble a continuous structure (Figure 3a, c, e). So, the formed adsorption film is very smooth. In the ink with poor solvent, the ion-adsorption nanoparticles will congregate and precipitate in the form of big particle (Figure 3b, d, f). Accordingly, the adsorption film is very coarse.

The relationship between the adhesion of the conductive patterns and the solvent used in the functional ink is listed in
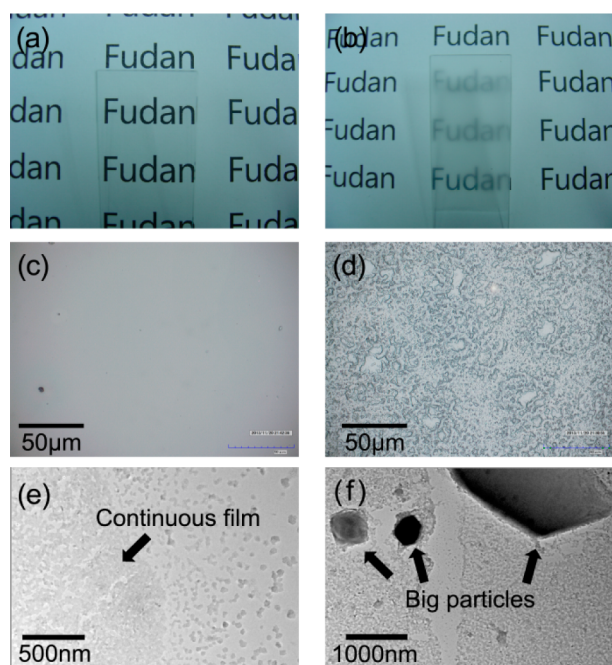
Figure 3. (a, c, e) Morphology of the adsorption film using the solvent of butanol:2-methoxy ethanol = 1:2. The images are taken by (a) the camera, (c) the optical microscope, and (e) the TEM. The film is transparent with a very smooth surface. Only continuous film crystal phase can be found. (b, d, f) Morphology of the adsorption film with the solvent of butanol:2-methoxy ethanol:butyl acetate = 1:2:3. The images are taken by (b) the camera, (d) the optical microscope, and (f) the TEM. The film is semitransparent, and the magnified image indicates that the surface is coarse. The TEM image proves that many big particle crystals exist.

Table 1. The mixed solvents with good solvent (butanol, 2-methoxy ethanol) and poor solvent (butyl acetate) were used

Table 1. Relationship between the Adhesion of the Conductive Patterns and the Solvent Used in the Functional Ink

solvent	surface roughness of the adsorption film (μm)	adhesion[a]
butanol:2-methoxy ethanol = 1:2	0.001	0B
butanol:2-methoxy ethanol:butyl acetate = 1:2:1	0.027	0B
butanol:2-methoxy ethanol:butyl acetate = 1:2:3	0.269	5B
butanol:2-methoxy ethanol: butyl acetate = 1:2:6	0.471	0B

[a]The adhesion of the conductive patterns was measured following the standard ASTM D3359. 0B is the worst, 5B is the best. The electroless plating temperature is 40 °C and the plating time is 15 min.

(the effect of the mixed solvent to the PET substrate is shown in Figure S2 in the Supporting Information). The boiling point of butanol (117.5 °C) and 2-methoxy ethanol (124.5 °C) is lower than butyl acetate (126.5 °C). Therefore, the evaporation rate of butyl acetate is lower. In the functional ink with mixed solvent, nanoparticles will crystallize in the continuous film crystal phase at first. With the evaporation of good solvent, the residual solvent become poor to the nanoparticles. Hence, the big particle crystal phase is generated. So, the adsorption film deposited from mixed solvent is composed of two different crystal structures. The continuous film crystal phase can act as the binder, thus the adsorption film can adhere to the substrate. The big particle crystal phase is powdered without stickiness and can raise the surface roughness. The adsorption film formed from good solvent has a small surface roughness, resulting in the poor adhesion of the conductive patterns (Figure 3a, c). With the adding of butyl acetate, the surface roughness of the adsorption film increases correspondently. When the ratio of good solvent to poor solvent is 1:1, the adhesion of the conductive patterns can reach 5B (Figure 3b, d) (the test sample is shown in Figure S3 in the Supporting Information). However, the adhesion gets a sharp decline with 2/3 butyl acetate in the mixed solvent. That is because the continuous film crystal phase is inadequate, inducing the poor adhesion of the adsorption film with PET substrate.

Ion Adsorption. The adsorption film before and after ion adsorption was characterized by XPS (Figure 4a). The peaks at 368.3 and 374.3 eV after ion adsorption are ascribed to Ag 3d$_{5/2}$ and Ag 3d$_{3/2}$, proving the adsorption of silver ion. The peaks at 163.2 eV (before ion adsorption) and 162.4 eV (after ion adsorption) are assigned to mercapto groups. Additional XPS images can be seen in Figure S4 and S5 in the Supporting Information, elements contents in adsorption film can be seen in Figure S6 in the Supporting Information. Figure 4b demonstrates the FTIR of the adsorption film. The main difference before and after ion adsorption is the peak around 1372 cm^{-1}, which is ascribed to the stretching vibration of NO$_3^-$. The adsorbed silver ion exists in the form of silver-amine ion. This electropositive ion can attract NO$_3^-$ negative ion via Coulomb force. The bands at 3276, 3167 cm^{-1} (before ion adsorption) and 3267, 3161 cm^{-1} (after ion adsorption) are assigned to the asymmetric and symmetric stretching of NH$_2$. The silver ion can strengthen the stretching vibration of
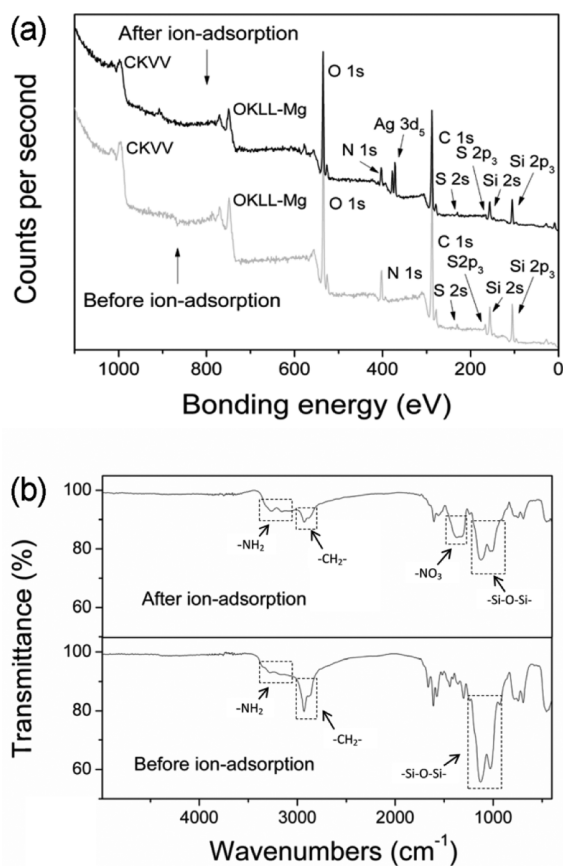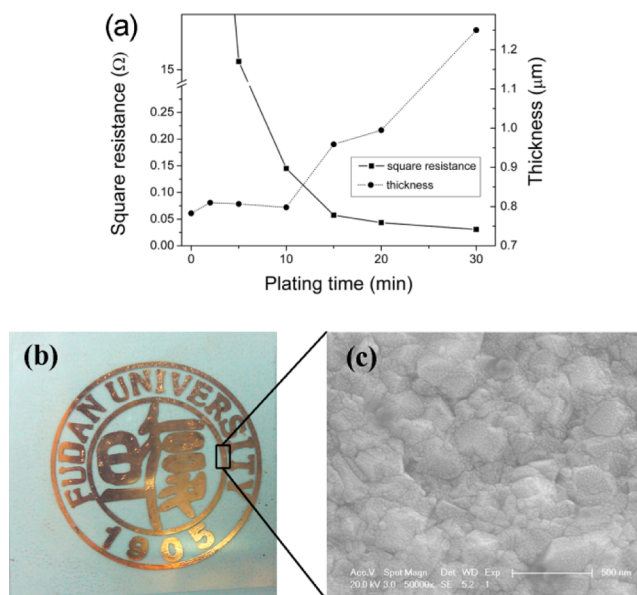
Figure 4. (a) XPS and (b) FTIR images of the adsorption film before and after adsorbing silver ion.

Figure 5. (a) Relationship between plating time with square resistance and thickness of the patterns. (b) Photo and (c) SEM images of the copper patterns fabricated by the PAP process.

coordinated NH$_2$, so the peaks after ion adsorption are sharper.[37,38]

Properties of the Conductive Patterns. The square resistance of the conductive patterns with different plating time is shown in figure 5a. The square resistance falls sharply and reaches 0.145 Ω at 10 min. Afterward the square resistance goes down slowly to 0.0308 Ω at 30 min. The plating time and square resistance are in inverse proportion, agreeing well with theoretic calculation. The thickness of the copper patterns is also exhibited in Figure 5a. Before electroless plating, the thickness is 0.783 μm. However, no obvious change is found before 10 min, indicating that copper is initially deposited inside the adsorption film. This phenomenon to some extent improves the adhesion of the deposited copper. 10 min later, copper starts to grow on the surface of the adsorption film with a rate of 0.0216 μm/min. The resistivity of the deposited copper is calculated to be 1.76×10^{-6} Ω cm (20 °C, the calculation process is listed in the Supporting Information and the temperature induced change of resistivity is shown in Figure S7 in the Supporting Information), very close to cubic copper (1.68×10^{-6} Ω cm, 20 °C).[39] After conservation at dry and enclosed environment for three months, the value remains unchanged.

The optical image of the prepared sample is displayed in Figure 5b. Additional optical images of the copper patterns can be seen in Figures S8, S9, and S10 in the Supporting Information. The resolution of the patterns is related to the method of patterning. The modified office inkjet printer can print the line as thin as 100 μm. Finer line can be achieved by better printer. The SEM image (Figure 5c) indicates that the conductive patterns are compact and continuous without void or crack. It can explain the excellent conductivity of the deposited copper.

CONCLUSIONS

A novel PAP process to fabricate conductive patterns is developed. The main steps include inkjet printing of the ion-adsorption functional ink, ion adsorption of catalytic ion, and electroless plating of copper. A novel ion-adsorption nanoparticle functional ink was prepared. Silver ion can coordinate with the amino groups on the nanoparticles, and thus be adsorbed to the substrate. Introducing Mercapto groups increased the stability of the adsorption film. Mixed solvent was used in the functional ink to increase the surface roughness of the adsorption film, resulting in an improved adhesion of the deposited copper. The resistivity of the copper patterns is about the same with bulk copper, and the adhesion is also excellent. In general, this cost-effective and pollution-decreased process can to some extent substitutes the traditional process, especially in the manufacture of FPC.

ASSOCIATED CONTENT

ⓢ Supporting Information

Size distribution of the ion-adsorption nanoparticles, the PET substrate before and after dipping in the solvent, the prepared copper patterns before and after tape test, XPS analysis of the adsorption layer, the relationship between temperature and the resistance of the copper patterns, optical microscope images and photos of the conductive patterns, and the calculation process of the resistivity of the deposited copper. This material is available free of charge via the Internet at http://pubs.acs.org.

AUTHOR INFORMATION

Corresponding Author

*E-mail: zgyang@fudan.edu.cn. Tel: +86-21-65642523. Fax: +86-21-65103056.

REFERENCES

(1) Teng, K. F.; Vest, R. W. *IEEE Trans. Compon. Hybrids Manuf. Technol.* **1987**, *10*, 545−549.

(2) Berggren, M.; Nilsson, D.; Robinson, N. D. *Nat. Mater.* **2007**, *6*, 3−5.

(3) Li, Y. N.; Wu, Y. L.; Ong, B. S. *J. Am. Chem. Soc.* **2005**, *127*, 3266−3267.

(4) Lee, Y. I.; Choi, J. R.; Lee, K. J.; Stot, N. E.; Kim, D. H. *Nanotechnology* **2008**, *19*, 415604.

(5) Lee, K. J.; Jun, B. H.; Kim, T. H.; Joung, J. W. *Nanotechnology* **2006**, *17*, 2424−2428.

(6) Perelaer, J.; Smith, P. J.; Mager, D.; Soltman, D.; Volkman, S. K.; Subramanian, V.; Korvink, J. G.; Schubert, U. S. *J. Mater. Chem.* **2010**, *20*, 8446−8453.

(7) Wu, Y. L.; Li, Y. N.; Ong, B. S. *J. Am. Chem. Soc.* **2007**, *129*, 1862−1863.

(8) Subramanain, V.; Frechet, J. M. J.; Chang, P. C.; Huang, D. C.; Lee, J. B.; Molesa, S. E.; Murphy, A. R.; Redinger, D. R.; Volkman, S. K. *Proc. IEEE* **2005**, *93*, 1330−1338.

(9) Lim, J. H.; Shim, J. H.; Choi, J. H.; Joom, J. H.; Park, K.; Jeon, H.; Moon, M. R.; Jung, D. G.; Kim, H. S.; Lee, H. J. *Appl. Phys. Lett.* **2009**, *95*, 012108.

(10) Calvert, P. *Chem. Mater.* **2001**, *13*, 3299−3305.

(11) Gans, B. J.; Duineveld, P. C.; Schubert, U. S. *Adv. Mater.* **2004**, *16*, 203−213.

(12) Kim, D. J.; Lee, S. H.; Jeong, S. H.; Moon, J. H. *Electrochem. Solid-State Lett.* **2009**, *12*, H195−H197.

(13) Ko, S. H.; Pan, H.; Grigoropoulos, C. P.; Luscombe, C. K.; Frechet, J. M. J.; Poulikakos, D. *Nanotechnology* **2007**, *18*, 345202.

(14) Kang, J. S.; Kim, H. S.; Ryu, J. G.; Hahn, H. T.; Jang, S. H.; Joung, J. W. *J. Mater. Sci: Mater. Electron.* **2010**, *21*, 1213−1220.

(15) Tai, Y. L.; Yang, Z. G. *J. Mater. Chem.* **2011**, *21*, 5938−5943.

(16) Reinhold, I.; Hendriks, C. E.; Eckardt, R.; Kranenburg, J. M.; Perelaer, J.; Baumann, R. R.; Schubert, U. S. *J. Mater. Chem.* **2009**, *19*, 3384−3388.

(17) Jeong, S. H.; Woo, K. H.; Kim, D. J.; Kim, S. K.; Kim, J. S.; Shin, H. J.; Xia, Y. N.; Moon, J. H. *Adv. Funct. Mater.* **2008**, *18*, 679−686.

(18) Chang, Y.; Wang, D. Y.; Tai, Y. L.; Yang, Z. G. *J. Mater. Chem.* **2012**, *22*, 25296−25301.

(19) Dearden, A. L.; Smith, P. J.; Shin, D. Y.; Reis, N.; Derby, B.; Òbrien, P. *Macromol. Rapid Commun.* **2005**, *26*, 315−318.

(20) Tseng, C. C.; Chang, C. P.; Sung, Y.; Chen, Y. C.; Ger, M. D. *Colloid. Surface. A* **2009**, *339*, 206−210.

(21) Kao, C. Y.; Chou, K. S. *Electrochem. Solid-State Lett.* **2007**, *10*, D32−D34.

(22) Shah, P.; Kervrekidis, Y.; Benziger, J. *Langmuir* **1999**, *15*, 1584−1587.

(23) Chen, W. D.; Lin, Y. H.; Chang, C. P.; Liu, Y. M.; Ger, M. D. *Surf. Coat. Technol.* **2011**, *205*, 4750−4756.

(24) Horiuchi, S.; Nakao, Y. *Surf. Coat. Technol.* **2010**, *204*, 3811−3817.

(25) Liao, Y. C.; Kao, Z. K. *ACS Appl. Mater. Inter.* **2012**, *4*, 5109−5113.

(26) Byeon, J. H.; Park, J. H.; Yoon, K. Y.; Hwang, J. H. *Langmuir* **2008**, *24*, 5949−5954.

(27) Zabetakis, D.; Dressick, W. J. *ACS Appl. Mater. Inter.* **2012**, *4*, 2358−2368.

(28) Cheng, K.; Yang, M. H.; Chiu, W. W. W.; Huang, C. Y.; Chang, J.; Ying, T. F.; Yang, Y. *Macromol. Rapid Commun.* **2005**, *26*, 247−264.

(29) Wang, C. W.; Yang, M. H.; Lee, Y. Z.; Cheng, K. *J. Imaging Sci. Technol.* **2007**, *51*, 452−455.

(30) Tseng, C. C.; Chou, Y. H.; Hsieh, T. W.; Wang, M. W.; Shu, Y. Y.; Ger, M. D. *Colloid. Surface. A* **2012**, *492*, 45−52.

(31) Su, W.; Li, P. Y.; Yang, F.; Liang, L. F.; Huo, L. N.; Tang, H. *React. Funct. Polym.* **2011**, *71*, 943−947.

(32) Garcia, A.; Maris, J. P.; Viel, P.; Palacin, S.; Berthelot, T. *Adv. Funct. Mater.* **2011**, *21*, 2096−2102.

(33) Konishi, S.; Honsho, K.; Yanada, M.; Minami, I.; Kimura, Y.; Ikeda, S. J. *Sensor. Actuat. A* **2003**, *103*, 135−142.

(34) Azzaroni, O.; Zheng, Z. J.; Yang, Z. Q.; Huck, W. T. S. *Langmuir* **2006**, *22*, 6730−6733.

(35) Huang, S. C.; Tsao, T. C.; Chen, L. J. *J. Electrochem. Soc.* **2010**, *157*, 222−227.

(36) Lu, Y. X.; Xue, L. L.; Li, F. *Surf. Coat. Technol.* **2010**, *205*, 519−524.

(37) Peard, W. J.; Pflaum, R. T. *J. Am. Chem. Soc.* **1958**, *80*, 1593−1596.

(38) Manna, A.; Imae, T.; Iida, M.; Hisamatsu, N. *Langmuir* **2001**, *37*, 6000−6004.

(39) Weast, R. C. *CRC Handbook of Chemistry and Physics*; CRC Press: Boca Raton, FL, 1984.

772

dx.doi.org/10.1021/am405539r | *ACS Appl. Mater. Interfaces* 2014, 6, 768−772